

## The appearance of Ti3+ states in solution-processed TiOx buffer layers in inverted organic photovoltaics

Ivan S. Zhidkov, John A. McLeod, Ernst Z. Kurmaev, Michael A. Korotin, Andrey I. Kukharenko, Achilleas Savva, Stelios A. Choulis, Danila M. Korotin, and Seif O. Cholakh

Citation: *Applied Physics Letters* **109**, 022108 (2016); doi: 10.1063/1.4958892

View online: <http://dx.doi.org/10.1063/1.4958892>

View Table of Contents: <http://scitation.aip.org/content/aip/journal/apl/109/2?ver=pdfcov>

Published by the [AIP Publishing](#)

---

### Articles you may be interested in

[The action mechanism of TiO<sub>2</sub>:NaYF<sub>4</sub>:Yb<sup>3+</sup>, Tm<sup>3+</sup> cathode buffer layer in highly efficient inverted organic solar cells](#)

*Appl. Phys. Lett.* **105**, 053301 (2014); 10.1063/1.4892472

[TiOx/Al bilayer as cathode buffer layer for inverted organic solar cell](#)

*Appl. Phys. Lett.* **103**, 173303 (2013); 10.1063/1.4826562

[Enhancement of inverted polymer solar cells with solution-processed ZnO-TiOX composite as cathode buffer layer](#)

*Appl. Phys. Lett.* **100**, 213906 (2012); 10.1063/1.4722800

[Cathode buffer layers based on vacuum and solution deposited poly\(3,4-ethylenedioxythiophene\) for efficient inverted organic solar cells](#)

*Appl. Phys. Lett.* **100**, 183301 (2012); 10.1063/1.4709481

[Performance improvement of polymer solar cells by using a solution processible titanium chelate as cathode buffer layer](#)

*Appl. Phys. Lett.* **91**, 023509 (2007); 10.1063/1.2757125

---

A promotional banner for Applied Physics Reviews. On the left is a small image of the journal cover, showing a 3D schematic of a device structure. The main background is a dark blue gradient with a bright light source on the right, creating a lens flare effect. The text 'NEW Special Topic Sections' is prominently displayed in white. Below this, 'NOW ONLINE' is written in yellow, followed by the title 'Lithium Niobate Properties and Applications: Reviews of Emerging Trends' in white. The AIP Applied Physics Reviews logo is in the bottom right corner.

**NEW Special Topic Sections**

**NOW ONLINE**  
Lithium Niobate Properties and Applications:  
Reviews of Emerging Trends

**AIP** Applied Physics  
Reviews

## The appearance of $Ti^{3+}$ states in solution-processed $TiO_x$ buffer layers in inverted organic photovoltaics

Ivan S. Zhidkov,<sup>1,2</sup> John A. McLeod,<sup>3,a)</sup> Ernst Z. Kurmaev,<sup>1,2</sup> Michael A. Korotin,<sup>1</sup> Andrey I. Kukhareenko,<sup>1,2</sup> Achilleas Savva,<sup>4</sup> Stelios A. Choulis,<sup>4</sup> Danila M. Korotin,<sup>1,2</sup> and Seif O. Cholakh<sup>2</sup>

<sup>1</sup>*M. N. Mikheev Institute of Metal Physics, Russian Academy of Sciences-Ural Branch, S. Kovalevskoi Str. 18, 620990 Yekaterinburg, Russia*

<sup>2</sup>*Institute of Physics and Technology, Ural Federal University, Mira Str. 19, 620002 Yekaterinburg, Russia*

<sup>3</sup>*Institute of Functional Nano and Soft Materials (FUNSOM), Jiangsu Key Laboratory for Carbon-Based Functional Materials and Devices, Soochow University, 199 Ren'ai Road, Suzhou, 215123, Jiangsu, People's Republic of China*

<sup>4</sup>*Molecular Electronics and Photonics Research Unit, Department of Mechanical Engineering and Materials Science and Engineering, Cyprus University of Technology, Kitiou Kiprianou Str. 45, 3603 Limassol, Cyprus*

(Received 19 February 2016; accepted 4 July 2016; published online 14 July 2016)

We study the low-temperature solution processed  $TiO_x$  films and device structures using core level and valence X-ray photoelectron spectroscopy (XPS) and electronic structure calculations. We are able to correlate the fraction of  $Ti^{3+}$  present as obtained from Ti 2p core level XPS with the intensity of the defect states that appear within the band gap as observed with our valence XPS. Constructing an operating inverted organic photovoltaic (OPV) using the  $TiO_x$  film as an electron selective contact may increase the fraction of  $Ti^{3+}$  present. We provide evidence that the number of charge carriers in  $TiO_x$  can be significantly varied and this might influence the performance of inverted OPVs. *Published by AIP Publishing.*  
[\[http://dx.doi.org/10.1063/1.4958892\]](http://dx.doi.org/10.1063/1.4958892)

Metal oxides are of increasing interest as materials for opto-electronic devices, and have been extensively used as functional layers in organic photovoltaics (OPVs). Among these metal oxides, solution processed titanium oxide ( $TiO_x$ ) is of particular interest as an electron acceptor/collector due to its low cost, facile synthesis, long-term stability, and a conduction band minima that is low enough in energy to accept/collect electrons from most organic semiconductors.<sup>1,2</sup>

Currently, the most popular use of  $TiO_x$  is as an electron selective contact in an inverted OPV architecture.<sup>2</sup> An inverted OPV has the cathode on the bottom and the anode on the top, and requires highly transparent and conductive materials for efficient operation—a role that can be fulfilled with  $TiO_x$ .<sup>3</sup> There are, however, open questions relevant to device performance, and related to the functionality of the  $TiO_x$  layer, that stem from uncertainties in the chemical composition and electronic structure of  $TiO_x$ . In this letter we study an inverted OPV device structure with a  $TiO_x$  electron selective contact using core level and valence X-ray photoelectron spectroscopy (XPS). There have been previous core level XPS<sup>4–6</sup> and computational<sup>7</sup> studies on the electronic structures of  $TiO_x$ . A combined core level and valence XPS study is of particular value as the valence spectra can be directly compared with electronic structure calculations, allowing the relationship between core level features and valence electronic structure to be explored. Previous experimental studies of the valence band in  $TiO_2$  have focused on isolated defects on otherwise pristine surfaces of single crystal;<sup>8</sup> herein, we focus on

an actual solution processed inverted OPV  $TiO_x$  buffer layer prepared by the sol-gel method.

The differences in the electronic structure between stoichiometric  $TiO_2$  and  $TiO_x$  seem to be primarily due to oxygen vacancies,<sup>7</sup> although excess interstitial Ti has also been suggested.<sup>8</sup> The most noticeable differences are the presence of  $Ti^{3+}$ ,<sup>5</sup> and the appearance of occupied states within the band gap.<sup>8</sup> OPVs with  $TiO_x$  have been reported with  $Ti^{3+}$  fractions ranging from near 0% (undetectable  $Ti^{3+}$  content) to 27%.<sup>6,9–11</sup> A previous study using nanocrystalline  $TiO_x$  in dye-sensitized solar cells (DSSCs) found that as the  $Ti^{3+}$  fraction increased, the device performance decreased.<sup>12</sup> However, no such correlation seems to exist in OPVs using  $TiO_x$  as an electron extraction layer. The wide range of  $Ti^{3+}$  content in these  $TiO_x$  films, and the lack of correlation between the  $Ti^{3+}$  content and the device performance highlights the need to understand the role of  $Ti^{3+}$  on the electronic structure of solution processed  $TiO_x$  films used as electron selective contacts in inverted OPVs.

$TiO_x$  films were prepared by doctor blading an ITO substrate with gel of titanium butoxide ( $C_{16}H_{36}O_4Ti$ ) dissolved in isopropanol and annealing at 140 °C for 25 min in air. One film was retained as-prepared for XPS characterization, and the other was used to fabricate an inverted OPV by adding subsequent layers of P3HT:PCBM ([6,6]-phenyl-C61-butyric acid methyl ester), PEDOT:PSS (poly(3,4-ethylenedioxythiophene) polystyrene sulfonate), and Ag as described elsewhere.<sup>9,13</sup> The inverted OPV exhibited diode-like behaviour under dark and illuminated conditions, as shown in Figure 1. We measured an open circuit voltage ( $V_{oc}$ ) of 0.591 V, a short-circuit current density ( $J_{sc}$ ) of 8.54 mA/cm<sup>2</sup>, a fill factor of 62%, and a photoconversion efficiency (PCE) of 3.14%. This

<sup>a)</sup> Author to whom correspondence should be addressed. Electronic mail: [jmcleod@suda.edu.cn](mailto:jmcleod@suda.edu.cn)

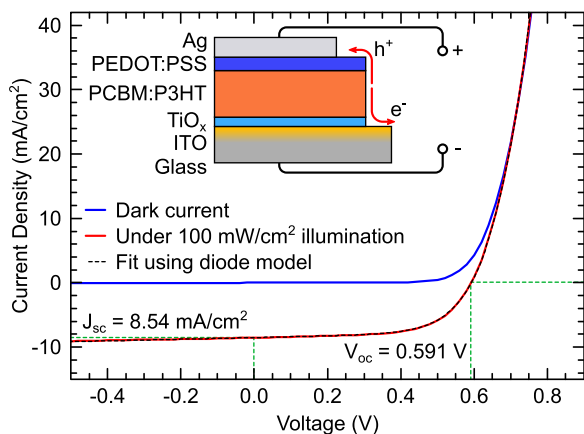


FIG. 1. Illuminated and dark current density–voltage curve for an ITO/TiO<sub>x</sub>/P3HT:PCBM/PEDOT:PSS/Ag inverted solar cell. A schematic of the solar cell is also shown.

performance was obtained after “soaking” the OPV under UV-light for 10 min; this step greatly improves the electron carrier selectivity and thus the inverted OPV device performance.<sup>14,15</sup>

The diode-like behaviour of this device is demonstrated by fitting the measured J-V curve to an equivalent circuit model<sup>16</sup> as described by Equation (1)

$$J = J_0 \left[ \exp\left(\frac{q(V - R_s J)}{nk_B T}\right) - 1 \right] - J_{ph} + \frac{V - R_s J}{R_{sh}}. \quad (1)$$

In Equation (1),  $J_{ph}$  is the photocurrent density,  $J_0$  is the reverse saturation current density,  $R_s$  is the series resistance,  $R_{sh}$  is the shunt resistance, and  $n$  is the ideality factor. The fitted values of  $J_{ph} = 8.5 \text{ mA/cm}^2$ ,  $J_0 = 0.98 \text{ } \mu\text{A/cm}^2$ ,  $R_s = 0.95 \text{ } \Omega\text{cm}^2$ ,  $R_{sh} = 790 \text{ } \Omega\text{cm}^2$ , and  $n = 2.6$  obtain an excellent match to the measured current density, as shown in Figure 1. Our ideality factor and reverse saturation current density are both larger, and our series resistance is considerably smaller, than those of a conventional P3HT:PCBM OPV.<sup>17</sup> The presence of a TiO<sub>x</sub> buffer layer may be responsible for these differences.

To measure the electronic structure of the TiO<sub>x</sub> layer in the inverted OPV, we use scotch tape to remove the Ag, PEDOT:PSS, and P3HT:PCBM layers, re-exposing the TiO<sub>x</sub>. XPS measurements were made using a PHI 5000 VersaProbe XPS spectrometer (ULVAC Physical Electronics, USA). This apparatus uses Al K $\alpha$  radiation (1486.6 eV) with a spot size of 100  $\mu\text{m}$ . The chamber pressure during measurements was better than  $10^{-7}$  Pa. Dual channel neutralization was used to compensate for local surface charge generated during the measurement. The XPS spectra are shown in Figure 2(a).

The Ti 2p XPS spectra are shown in Figure 2(b). There is the clear signature of Ti<sup>3+</sup> visible in the low-energy side of the Ti 2p<sub>3/2</sub> feature in both the as-prepared and extracted TiO<sub>x</sub> films. This feature is also present in the low-energy side of the Ti 2p<sub>1/2</sub> feature, although it is harder to see. The energy separation between the Ti<sup>3+</sup> and Ti<sup>4+</sup> 2p<sub>3/2</sub> and 2p<sub>1/2</sub> levels are both  $5.7 \pm 0.1 \text{ eV}$ , as previously reported.<sup>1,4,6,9,10</sup> The measured spectra can be accurately reconstructed with using a Shirley background and four fitted Voigt lineshapes corresponding to the 2p<sub>3/2</sub> and 2p<sub>1/2</sub> core levels of Ti<sup>3+</sup> and Ti<sup>4+</sup>. These fitted peaks are in excellent agreement with

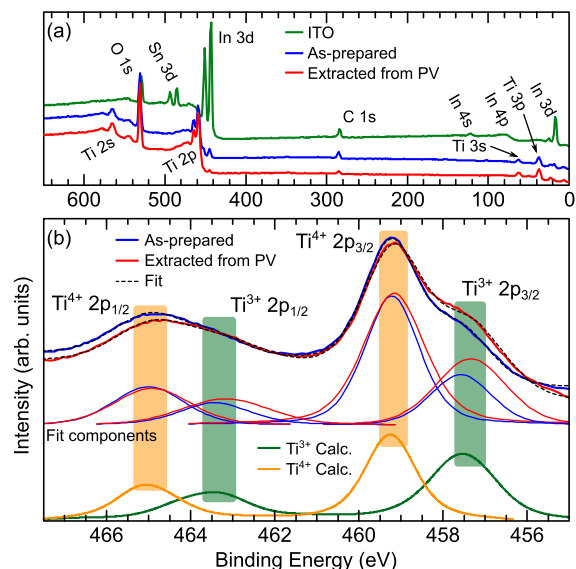


FIG. 2. The (a) survey and (b) Ti 2p XPS spectra TiO<sub>x</sub> films. All spectra were calibrated by setting the carbon impurity C 1s core level to 285.0 eV.<sup>18</sup>

simulated XPS spectra from octahedrally coordinated Ti<sup>3+</sup> and Ti<sup>4+</sup>, as shown in Figure 2. These simulations were performed using the CTM4XAS program<sup>19</sup> with a 10 Dq value of 2.1 eV and broadened to mimic the experimental resolution. We estimate the Ti<sup>3+</sup> fraction of the total Ti as  $33 \pm 1\%$  and  $39 \pm 1\%$  in the as-prepared and extracted TiO<sub>x</sub> films, respectively, using the area of the fitted XPS peaks.

There is negligible difference in the O 1s XPS spectra from both TiO<sub>x</sub> films, as shown in Figure 3(a). The O 1s XPS very clearly shows the O<sup>2-</sup> from TiO<sub>2</sub> at 530.0 eV, and the spectrum has a somewhat extended tail on the high-energy side. A previous report showed clear O 1s XPS features from Ti<sub>2</sub>O<sub>3</sub> and OH in a DSSC;<sup>12</sup> we do not observe these here. The high-energy tail in our O 1s XPS is likely due to a mixture of various carbon–oxygen complexes on the surface. This suspicion is verified by examining the C 1s XPS spectra from both TiO<sub>x</sub> films, as shown in Figure 3(b). Interestingly, the C 1s XPS of the extracted TiO<sub>x</sub> film is essentially identical to that of the as-prepared film, indicating that our scotch tape extraction of the TiO<sub>x</sub> film from the OPV removed all of the P3HT:PCBM. Most of the C 1s XPS can be attributed to C-C bonds, although a C-O=C structure and other carbon/oxygen complexes contribute to the high-energy tail of the main C 1s XPS peak.<sup>20</sup>

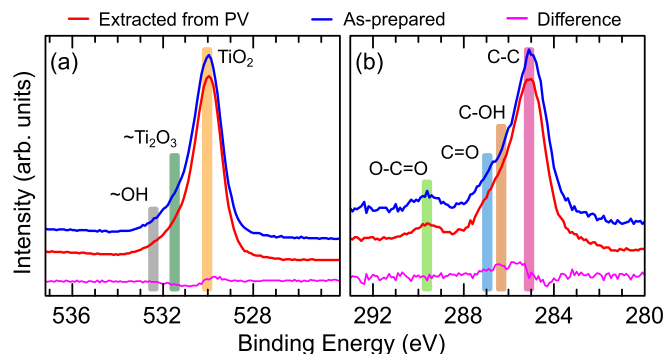


FIG. 3. The normalized (a) O 1s and (b) C 1s XPS spectra from the TiO<sub>x</sub> films. The difference between the two spectra is also shown.

The difference in the  $\text{Ti}^{3+}$  content of the as-prepared and extracted  $\text{TiO}_x$  films may have three possible origins: (1) it may simply highlight the variability in  $\text{TiO}_x$  stoichiometry even from films prepared from the same precursors, (2) the interaction between  $\text{TiO}_x$  and the P3HT:PCBM active layer in the OPV may remove oxygen from the  $\text{TiO}_x$  layer, (3) the UV soaking step may cause structural changes in the  $\text{TiO}_x$  leading to more surface  $\text{Ti}^{3+}$ . We expect that all three of these contribute to the  $\text{Ti}^{3+}$  content. Residual carbon from the titanium butoxide precursor or from the atmosphere may draw additional oxygen from the  $\text{TiO}_x$  film,<sup>5</sup> creating many O vacancies. The thermal annealing processing step may result in removing most of these C-O complexes from the surface (as well as surface -OH groups),<sup>6</sup> as the relatively weak C 1s XPS spectra suggest minimal carbon contamination. Adding (and subsequently removing) P3HT:PCBM may create even more O vacancies, while soaking under UV light may cause more interstitial Ti to migrate to the surface.<sup>8</sup> Both of these processes would increase the surface  $\text{Ti}^{3+}$  fraction, as observed in our XPS measurements of the extracted  $\text{TiO}_x$  film compared with the as-prepared  $\text{TiO}_x$  film. We note that the stoichiometries estimated from the XPS measurements are  $\text{TiO}_{1.8}$  and  $\text{TiO}_{1.6}$  for the as-prepared and extracted films, respectively (curve-fitting was employed to remove the non-Ti related features in the O 1s XPS, and we used the standard elemental sensitivity factors<sup>18</sup>). On the other hand, our two films exhibit substantial  $\text{Ti}^{3+}$  content, while other similar inverted OPVs exhibit significantly less  $\text{Ti}^{3+}$ .<sup>9</sup> It seems that the ambient conditions during device fabrication may have a significant influence on the  $\text{Ti}^{3+}$  content. Our findings regarding the two films studied herein may suggest, however, that the  $\text{Ti}^{3+}$  content in an inverted OPV will be slightly increased compared with an as-prepared  $\text{TiO}_x$  film which has not undergone UV soaking or had an active layer deposited on top but was prepared in the same batch as the OPV. This is an important possibility to consider, as previous XPS studies on OPVs have only examined as-prepared  $\text{TiO}_x$  films,<sup>1,4,6,9,12,21</sup> and have not extracted the  $\text{TiO}_x$  from the OPV after operation as we have done here.

Herein we adopt the coherent potential approximation (CPA) to calculate the electronic structure of  $\text{TiO}_x$ .<sup>22</sup> We start with the local density approximation (LDA) electronic structure of defect-free  $\text{TiO}_2$  (using a  $2 \times 2 \times 1$  supercell based on the experimental lattice parameters<sup>23</sup>) calculated using the Stuttgart TB-LMTO-ASA code (version 47).<sup>24</sup> The electronic structure of  $\text{TiO}_x$  is then obtained from the single-site electronic Green's function.

Our calculated valence band electronic density of states (DOS) using CPA is shown in Figure 4 to be in good agreement with our measured XPS spectra, and both reveal defect-related states within the band gap. The mid-gap defect states in our CPA calculation represent 2.1% of the total occupied states in the valence band, while the area under the defect feature is 2.6% and 2.8%, suggesting a stoichiometry of  $\text{TiO}_{1.85}$  and  $\text{TiO}_{1.83}$  and a  $\text{Ti}^{3+}$  fraction of 30% and 34%, in our as-prepared and extracted  $\text{TiO}_x$  films, respectively. This is in reasonable agreement with our estimates based on the Ti 2p XPS. As mentioned above, comparing the elemental sensitivity-weighted O 1s and Ti 2p XPS intensities gives us  $\text{TiO}_{1.8}$  and  $\text{TiO}_{1.6}$  for the as-prepared and extracted  $\text{TiO}_x$

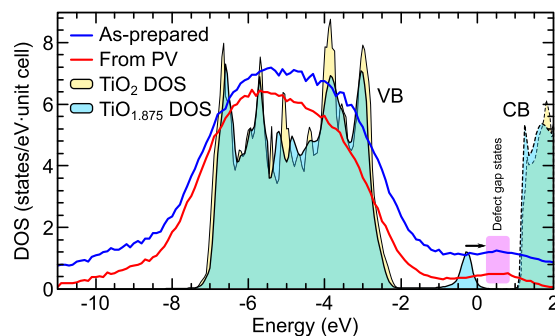


FIG. 4. Valence XPS spectra (Shirley background subtracted) of  $\text{TiO}_x$  films and calculated electronic DOS. The top of the valence band is set to 0 eV.

films, respectively. It therefore seems likely that some of the  $\text{Ti}^{3+}$  is also due to interstitial Ti.<sup>8</sup> Note that interstitial  $\text{Ti}^{3+}$  is expected to contribute negligible mid-gap states.<sup>25</sup>

We can estimate the number of free electrons at room temperature as  $N_d \exp(-\frac{E_c - E_F}{k_B T}) \approx 4 \times 10^{17} \text{ cm}^{-3}$  in our  $\text{TiO}_x$  films, where  $N_d$  is the number of states in the defect band,  $E_c = 1 \text{ eV}$  is the conduction band minimum, and  $E_F \approx 0.75 \text{ eV}$  based on the XPS defect gap states shown in Figure 4. This is a fairly substantial level of doping and may greatly enhance the carrier transport in the  $\text{TiO}_x$  films reported herein compared with stoichiometric  $\text{TiO}_2$ . This may be the origin of the relatively large reverse saturation current and relatively low series resistance observed in the inverted OPVs under investigation.

To summarize, we have studied the electronic structure of  $\text{TiO}_x$  in an inverted OPV device using core level and valence XPS and density functional theory (DFT)-CPA calculations. We found that the  $\text{Ti}^{3+}$  fraction can be obtained from the Ti 2p XPS core level or the total area of the mid-gap states in the valence XPS. The quantity of  $\text{Ti}^{3+}$  likely depends on the method of synthesis, exposure to oxygen, and UV light-soaking. If these can be carefully controlled, there is the potential for engineering the  $\text{Ti}^{3+}/\text{Ti}^{4+}$  ratio. This is important since the quantity of  $\text{Ti}^{3+}$  can have a major influence on the availability of free electrons in the  $\text{TiO}_x$  films.

A final question remains: What is the effect of  $\text{Ti}^{3+}$  on an OPV device? Compared with  $\text{TiO}_x$ -based DSSCs or  $\text{TiO}_x$  + P3HT-based OPVs,  $J_{sc}$  and  $V_{oc}$  for  $\text{TiO}_x$  + P3HT:PCBM-based OPVs are quite consistent, as shown in Fig. 5(a). However, this does not mean that  $\text{Ti}^{3+}$  has no influence on the OPV. For example, we previously reported at  $\text{TiO}_x$  OPV with a PCE of 3.06% and a  $\text{Ti}^{3+}$  fraction of roughly 5%.<sup>9</sup>

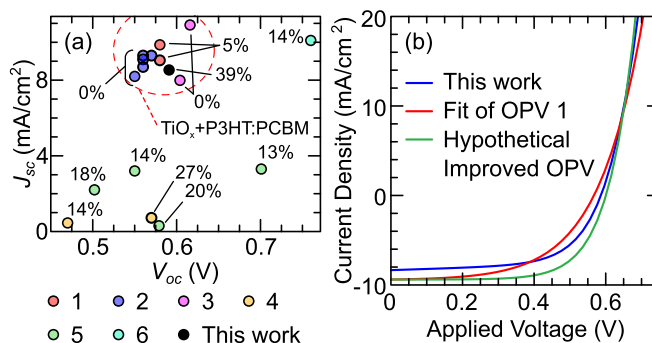


FIG. 5. (a)  $J_{sc}$  and  $V_{oc}$  for several  $\text{TiO}_x$ -based OPVs (1,<sup>9</sup> 2,<sup>6</sup> 3,<sup>4</sup> 4<sup>1</sup>) and DSSCs (5,<sup>12</sup> 6<sup>21</sup>). The  $\text{Ti}^{3+}$  fraction is labelled. (b) The fitted diode-model current density-voltage curves from this work,  $\text{TiO}_x$  OPV 1,<sup>9</sup> and a hypothetical OPV using the best parameters of the two.

The J-V curve from this OPV can be accurately fit using the diode model (see Fig. 5(b)). Our previous OPV exhibits a better  $J_{ph}$  and  $R_{sh}$ , while our present OPV exhibits a better  $J_0$  and a better  $n$ . Increasing  $Ti^{3+}$  content may improve the diode-behaviour of the OPV while simultaneously decreasing the parallel resistance. However if, through carefully engineering the  $TiO_x$  layer, one could obtain an OPV with the good diode characteristics of the latter and the good resistance characteristics of the former, this improved OPV would exhibit an increased PCE of 3.9% (see Fig. 5(b)). This is admittedly speculative, but we do expect that increased  $Ti^{3+}$  content will have both good and bad effects on the device, and we anticipate that careful engineering of the  $TiO_x$  layer may improve device efficiency. There is, therefore, good reason to investigate engineering the  $Ti^{3+}$  content in  $TiO_x$  electron-selective contacts in OPVs.

This research was done with partial support from the Government of the Russian Federation (Act 211, Agreement No. 02.A03.21.0006), the European Regional Development Fund, and the Republic of Cyprus through the Research Promotion Foundation (Strategic Infrastructure Project NEA ΥΠΟΔΟΜΗ/ΣΤΡΑΤΗ/0308/06), the National Natural Science Foundation of China (Project No. 11404232), and the China Postdoctoral Science Foundation (Project No. 2014M551645). The CPA calculations were supported by the Russian Science Foundation (Project No. 14-22-00004).

<sup>1</sup>H. Kang, C. Lee, S. C. Yoon, C.-H. Cho, J. Cho, and B. J. Kim, *Langmuir* **26**, 17589 (2010).

<sup>2</sup>C. Waldauf, M. Morana, P. Denk, P. Schilinsky, K. Coakley, S. A. Choulis, and C. J. Brabec, *Appl. Phys. Lett.* **89**, 233517 (2006).

<sup>3</sup>A. Savva and S. A. Choulis, *Appl. Phys. Lett.* **102**, 233301 (2013).

<sup>4</sup>X. Bao, L. Sun, W. Shen, C. Yang, W. Chen, and R. Yang, *J. Mater. Chem. A* **2**, 1732 (2014).

<sup>5</sup>J. Yu, J. Yu, W. Ho, Z. Jiang, and L. Zhang, *Chem. Mater.* **14**, 3808 (2002).

<sup>6</sup>R. Peng, F. Yang, X. Ouyang, Y. Liu, Y.-S. Kim, and Z. Ge, *Appl. Phys. A* **114**, 429 (2014).

<sup>7</sup>N. A. Deskins, R. Rousseau, and M. Dupuis, *J. Phys. Chem. C* **115**, 7562 (2011).

<sup>8</sup>S. Wendt, P. T. Sprunger, E. Lira, G. K. H. Madsen, Z. Li, J. Ø. Hansen, J. Matthiesen, A. Blekinge-Rasmussen, L. Erik, B. Hammer, and F. Besenbacher, *Science* **320**, 1755 (2008).

<sup>9</sup>A. Savva, F. Petraki, P. Eleftheriou, L. Sygellou, M. Voigt, M. Giannouli, S. Kennou, J. Nelson, D. D. C. Bradley, C. J. Brabec, and S. A. Choulis, *Adv. Energy Mater.* **3**, 391 (2013).

<sup>10</sup>S. Avasthi, W. E. McClain, G. Man, A. Kahn, J. Schwartz, and J. C. Sturm, *Appl. Phys. Lett.* **102**, 203901 (2013).

<sup>11</sup>Z. Lin, C. Jiang, C. Zhu, and J. Zhang, *ACS Appl. Mater. Interfaces* **5**, 713 (2013).

<sup>12</sup>Y. Yu, K. Wu, and D. Wang, *Appl. Phys. Lett.* **99**, 192104 (2011).

<sup>13</sup>A. Savva, M. Neophytou, C. Koutsides, K. Kalli, and S. A. Choulis, *Org. Electron.* **14**, 3123 (2013).

<sup>14</sup>R. Steim, S. A. Choulis, P. Schilinsky, and C. J. Brabec, *Appl. Phys. Lett.* **92**, 093303 (2008).

<sup>15</sup>T. Kuwabara, C. Iwata, T. Yamaguchi, and K. Takahashi, *ACS Appl. Mater. Interfaces* **2**, 2254 (2010).

<sup>16</sup>C. Waldauf, M. C. Scharber, P. Schilinsky, J. A. Hauch, and C. J. Brabec, *J. Appl. Phys.* **99**, 104503 (2006).

<sup>17</sup>C. Waldauf, P. Schilinsky, J. Hauch, and C. J. Brabec, *Thin Solid Films* **451–452**, 503 (2004).

<sup>18</sup>J. Moulder, W. Stickle, P. Sobol, and K. Bomben, *Handbook of X-ray Photoelectron Spectroscopy*, edited by J. Chastain (Perkin-Elmer Corporation, Physical Electronics Division, 1992), p. 261.

<sup>19</sup>E. Stavitski and F. M. de Groot, *Micron* **41**, 687 (2010).

<sup>20</sup>D. T. Clark, B. J. Cromarty, and A. Dilks, *J. Polym. Sci.* **16**, 3173 (1978).

<sup>21</sup>S. Pan, X. Liu, M. Guo, S. F. Yu, H. Huang, H. Fan, and G. Li, *J. Mater. Chem. A* **3**, 11437 (2015).

<sup>22</sup>M. A. Korotin, N. A. Skorikov, V. M. Zainullina, E. Z. Kurmaev, A. V. Lukoyanov, and V. I. Anisimov, *JETP Lett.* **94**, 806 (2012).

<sup>23</sup>S. C. Abrahams and J. L. Bernstein, *J. Chem. Phys.* **55**, 3206 (1971).

<sup>24</sup>O. K. Andersen and O. Jepsen, *Phys. Rev. Lett.* **53**, 2571 (1984).

<sup>25</sup>C. Di Valentin, G. Pacchioni, and A. Selloni, *J. Phys. Chem. C* **113**, 20543 (2009).